Gold-Decorated Block Copolymer Microspheres with Controlled Surface Nanostructures

Minsoo P. Kim,[†] Dong Jin Kang,[†] Dae-Woong Jung,[‡] Aravindaraj G. Kannan,[†] Ki-Hyun Kim,[†] Kang Hee Ku,[†] Se Gyu Jang,[§] Weon-Sik Chae,[⊥] Gi-Ra Yi,[∥,*] and Bumjoon J. Kim[†,*]

[†]Department of Chemical and Biomolecular Engineering, Korea Advanced Institute of Science and Technology (KAIST), Daejeon 305-701, Republic of Korea, [‡]Department of Engineering Chemistry, Chungbuk National University, Cheongju, Chungbuk 361-763, Republic of Korea, [§]Materials Research Laboratory, University of California, Santa Barbara, California 93106, United States, [⊥]Gangneung Center, Korea Basic Science Institute, Gangneung 210-702, Republic of Korea, and [∥]Department of Polymer Science and Engineering, Sungkyunkwan University, Suwon, 440-746 Republic of Korea

ABSTRACT Gold-decorated block copolymer microspheres (BCP-microspheres) displaying various surface morphologies were prepared by the infiltration of Au precursors into polystyrene-*b*-poly(4-vinylpyridine) (PS-*b*-P4VP) microspheres. The microspheres were fabricated by emulsifying the PS-*b*-P4VP polymers in chloroform into a surfactant solution in water, followed by the evaporation of chloroform. The selective swelling of the P4VP domains in the microspheres by the Au precursor under acidic conditions resulted in the formation of Au-decorated BCP-microspheres with various surface nanostructures. As evidenced by transmission electron microscopy (TEM) and scanning electron microscopy (SEM) measurements, dotted surface patterns were formed when microspheres smaller than 800 nm were synthesized, whereas fingerprint-like surface patterns were observed with microspheres larger than 800 nm. Au nanoparticles (NPs) were located inside P4VP domains near the surfaces of the prepared microspheres, as confirmed by TEM. The optical properties of the BCP-microspheres were characterized using UV–vis absorption spectroscopy and fluorescence lifetime measurements. A maximum absorption peak was observed at approximately 580 nm, indicating that Au NPs are densely packed into P4VP domains on the microspheres. Our approach for creating Au-NP-hybrid BCP-microspheres can be extended to other NP systems such as iron-oxide or platinum NPs. These precursors can also be selectively incorporated into P4VP domains and induce the formation of hybrid BCP-microspheres with controlled surface nanostructures.

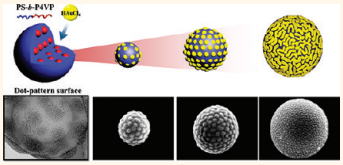

KEYWORDS: block copolymer · colloid particle · block copolymer microsphere · raspberry particle · surface nanostructure · Au nanoparticles

Using emulsion droplets to confine block copolymer (BCP) solutions in water, BCP colloidal particles can be produced as the solvent in the emulsion droplets evaporates. The nanostructures of these particles are unique and can be controlled by changing the volume fraction of blocks, the particle size, and the interfacial tension between each of the blocks and the particle interface.[1−3] For example, while onion-like particles were prepared using symmetric diblock copolymers, other nanostructured particles were prepared simply by adding low-molecular-weight homopolymers in different ratios.[1] In addition, it has been reported that the internal nanomorphology of BCPs in particles is significantly affected by block interactions with the particle surfaces (*i.e.*, controlling surfactants), and the overall colloidal particle shape changes during structural evolution as evaporation takes place.[3]

Functional nanoparticles (NPs) can be incorporated into such colloidal particles, using methods previously demonstrated in thin films,[4−7] to produce colloidal composite particles with complex internal nanophases. Several experimental methods have been developed to incorporate inorganic NPs into polymeric nanostructures, which can be categorized into so-called *ex situ* and *in situ* methods.[5,8−21] The *ex situ* approach exploits the cooperative self-organization of preformed NPs and BCPs. The strategy for incorporating and controlling the location of NPs in a BCP or polymer blend involves tuning the surface properties of the NPs by end-attaching ligands such as organic molecules,[5,22−24] homopolymers,[10,25−30] mixtures of homopolymers,[4,8] or copolymers[16,21,31−33] to the NP surfaces. In addition, a variety of NPs can be incorporated into a polymer matrix with a controlled positioning once they are coated with suitable ligands. Another popular approach involves the *in situ* synthesis of NPs within a BCP template using preformed micelles of BCPs that contain metal precursors.[9,11−14,17,34] In this method, one of the blocks should retain a strong affinity for metallic precursors. Such blocks include poly(2-vinylpyridine) (P2VP) and poly(4-vinylpyridine) (P4VP), whose nitrogen atoms

* Address correspondence to bumjoonkim@kaist.ac.kr (B.J.K.); yigira@skku.edu (G.-R.Y.).

Received for review January 14, 2012 and accepted February 21, 2012.

Published online February 21, 2012
10.1021/nn300194z

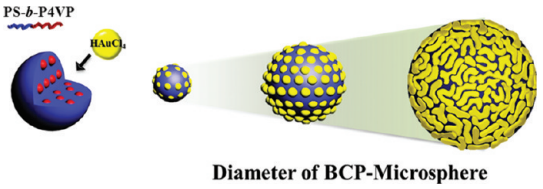

Scheme 1. Schematic illustration of metal hybrid BCP-microsphere with a controlled surface structure.

interact strongly with metal precursors.[6,7] Metal–polymer composite particles can be produced by the direct reduction of metallic precursors inside BCP micelles, *e.g.*, using a reducing agent or plasma treatment.[34–37] However, the *in situ* formation of metallic particles within submicrometer BCP colloidal particles has not been reported.

In this study, we have demonstrated a simple and facile method to produce metal hybrid "BCP-microspheres" with controlled surface nanostructures. First, microspheres of polystyrene-*b*-poly(4-vinylpyridine) (PS-*b*-P4VP) polymeric micelles were prepared by an emulsion encapsulation and shrinkage method. Then, upon the addition of Au precursors in acidic water, Au NPs formed only near the surfaces of these BCP-microspheres. Surprisingly, unique dot or fingerprint-like patterns on their surfaces evolved during metallization because P4VP domains were selectively swollen and migrated to the surfaces. The surface structures can be controlled by tuning the diameter of the BCP-microspheres. Thus, we successfully synthesized Au-NP-decorated BCP-microspheres and demonstrated the simultaneous control of their surface morphologies.

RESULTS AND DISCUSSION

For BCP-microspheres, a 1 wt % chloroform solution of PS-*b*-P4VP diblock copolymer was emulsified in water containing 1 wt % Pluronic F108 surfactant *via* high-intensity ultrasonic irradiation. Subsequently, through the evaporation of the chloroform, BCP-microspheres were produced, which were well dispersed in water, as shown in the optical micrograph of Figure 1a. The SEM image in Figure 1c shows BCP-microspheres with smooth surfaces. In contrast, after the microspheres were treated with the Au precursor ($HAuCl_4$) solution in water, they exhibited very rough surfaces covered with small hemispheres, as shown in Figure 1d. These surface structures were found to be uniform in size and ordered regularly. In addition, these transformed microspheres were well dispersed in water, as illustrated in the optical micrograph of Figure 1b.

To gain deeper insight into the morphological changes at the surface of the BCP-microspheres, the microspheres were characterized by surface and cross-sectional TEM images. For cross-sectional TEM measurements, the microspheres were first dropped onto an epoxy film and dried. Then, the samples were

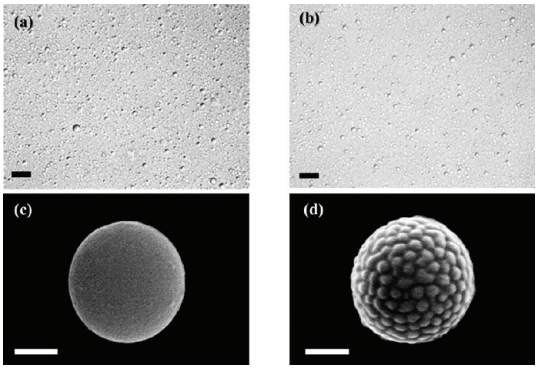

Figure 1. Optical images of PS-*b*-P4VP microsphere (a) before and (b) after inserting Au precursors. Scale bar is 10 μm. The PS-*b*-P4VP microspheres were well dispersed in water before and after adding Au precursors. SEM images of a PS-*b*-P4VP microsphere (c) before and (d) after adding Au precursors. Scale bar is 200 nm. The morphology of the microsphere changes from being spherical to adopting a dotted pattern upon the addition of Au precursors.

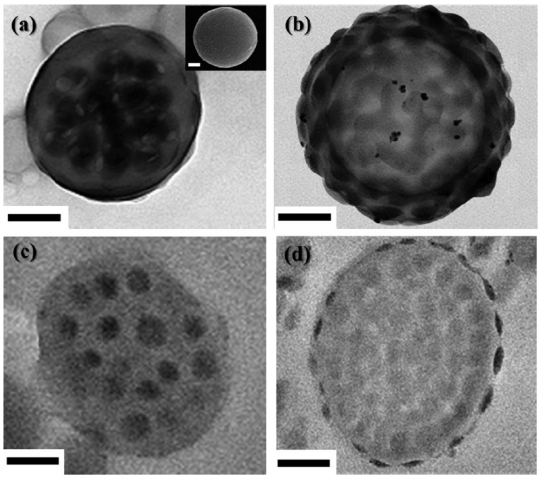

Figure 2. Surface TEM images of PS-*b*-P4VP microspheres (a) before and (b) after inserting Au precursor and their corresponding cross-sectional TEM images (c and d, respectively). Scale bars are 100 nm. The inset in part (a) shows a SEM image of the spherical microsphere before Au precursor infiltration, whereas (b) and (d) show Au-NP-incorporated P4VP domains on the outermost layer of the BCP-microsphere in black.

carefully microtomed at room temperature to yield a 50 nm thick film. As shown in Figure 2a and c, spherical micellar structures of PS-*b*-P4VP polymers with P4VP cores were observed in the microsphere. The P4VP cores in the micelles appear as dark regions in the microsphere due to the selective staining of P4VP chains by iodine vapor. It was found that the asymmetric PS-*b*-P4VP polymers with a high molecular weight (M_n = 262 kg/mol, f_{PS} = 0.76, polydispersity index(PDI) = 1.14) formed spherical micelles consisting of PS coronae and P4VP cores in a chloroform solution because chloroform has a much higher affinity for PS than for P4VP. It is known that the polymer–solvent interaction parameter between PS chains and

chloroform is 0.34, which is much lower than that between P4VP chains and chloroform (1.55).[38,39] The average P4VP core size of PS-*b*-P4VP micelles in the microspheres was estimated to be 47.5 ± 9.2 nm from the TEM image. This value agrees with the average P4VP core size (43.7 ± 3.1 nm) from the AFM measurement, where a PS-*b*-P4VP micellar film was prepared on Si substrate from 0.5 wt % PS-b-P4VP solution in chloroform. The AFM measurement (Figure S2) also provides an estimate of the average PS-*b*-P4VP micelle size from the center-to-center distance between two different P4VP micelle cores, which was found to be 59.5 ± 5.8 nm.

After the infiltration of the Au precursor into the BCP-microspheres, the surfaces of the BCP-microspheres were dramatically transformed, changing from smooth to dot-patterned surfaces. Figure 2b and d show surface and cross-sectional TEM images of the BCP-microspheres with dot-patterned surfaces, which were observed without iodine staining. The surface TEM image in Figure 2b shows a uniform arrangement of small hemispheres containing Au NPs on the microsphere surfaces, with structures resembling raspberries. This structure corresponds to the SEM image shown in Figure 1d. To examine the internal structures of the BCP-microspheres, cross-sectional TEM images of the microspheres were taken after microtoming. The TEM image in Figure 2d clearly demonstrates that the Au precursor infiltrated the P4VP domains only near the surfaces of the microspheres but not the P4VP domains inside the microspheres. The Au precursors could not reach the P4VP domain inside, because the P4VP domains inside were isolated by the PS matrix in the microspheres. The P4VP domains appear slightly darker than the PS matrix in Figure 2d because the electron scattering from P4VP polymers is stronger than that of PS polymers.[40]

In previous reports, raspberry-like particles were prepared by attaching premade NPs on spheres, which was typically based on chemical interactions between NPs and organic molecules on the sphere surfaces.[41,42] For instance, amino-functionalized ligands[43,44] on spheres were used to attach iron or silica NPs, while thiol-functionalized ligands[45] were used to interact with gold, silver, or copper NPs. However, in this approach, specific types of NPs and organic molecules on the sphere are required, which limits the types of raspberry-structured particles that are formed. Recently, a few researchers have prepared raspberry-like particles using self-assembled structures of BCP micelles with cross-linkable core units.[46,47] Similarly, our BCP-microspheres, which show dotted surface patterns, resemble raspberry-like structures. However, the mechanism of the formation of such raspberry particles is very different from that of the particles mentioned above. Our BCP-microspheres were formed based on the swelling and deswelling processes that occurred upon the selective incorporation of Au NPs with acidic water into P4VP domains.

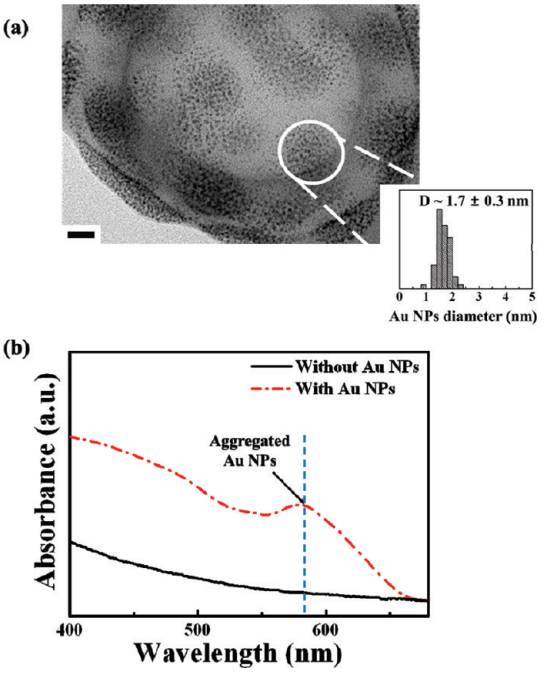

Figure 3. (a) TEM image of a Au-NP-decorated PS-*b*-P4VP microsphere. The Au NPs were selectively formed in the P4VP domains at the outermost layer of the microspheres. The corresponding histogram (inset) represents the diameter distribution of the Au NPs. Scale bar is 20 nm. (b) UV−vis absorbance spectroscopy of BCP-microspheres without (solid line) and with (dotted line) Au NPs. The absorption peak at the wavelength of 580 nm indicates the presence of densely packed Au NPs in the microspheres.

To characterize the Au NPs formed within the P4VP domains at the surface of the BCP-microspheres, both TEM and UV−vis spectroscopy were performed. The diameter distribution of the Au NPs was determined from the cross-sectional TEM image using image-analysis software; the inset in Figure 3a shows the diameter distribution of the Au NPs, which have an average diameter of 1.7 ± 0.3 nm. Moreover, the average diameter of the Au NPs remained constant regardless of the diameter of BCP-microsphere. To provide additional evidence of Au NP formation, the UV−vis absorption spectra of BCP-microspheres before and after treatment with Au precursor solution were compared as shown in Figure 3b. For the microspheres obtained after the incorporation of Au NPs, a maximum absorption peak at approximately 580 nm was observed, which is evidence of the presence of Au NPs. While it is well known that the absorption spectrum of Au NPs is highly sensitive to NP diameter,[48,49] the peak position (~580 nm) of the Au-NP-decorated BCP-microspheres is red-shifted compared to a typical absorbance peak (510−520 nm) of Au NPs with similar diameters in the solution.[50,51] On the other hand, when the Au NPs are sufficiently close to each other, the absorption peak can be shifted to a higher wavelength because the

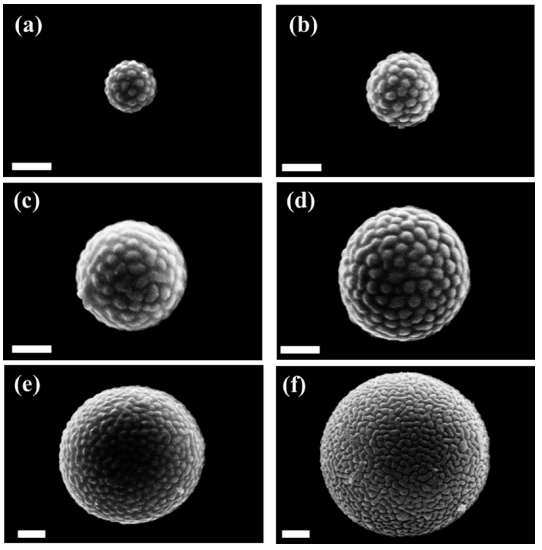

Figure 4. SEM images of Au-NP-decorated PS-*b*-P4VP microspheres with diameters of (a) 250 nm, (b) 360 nm, (c) 540 nm, (d) 640 nm, (e) 1020 nm, and (f) 1190 nm. Scale bar is 200 nm. These images clearly reveal that the P4VP domain structure incorporating the Au NPs on the microsphere depends on the microsphere diameter. The surface structure of BCP-microspheres smaller than 800 nm in diameter shows a discrete dot pattern. As the diameter of BCP-microsphere increases, the surface structure changes from a discontinuous to a continuous morphology.

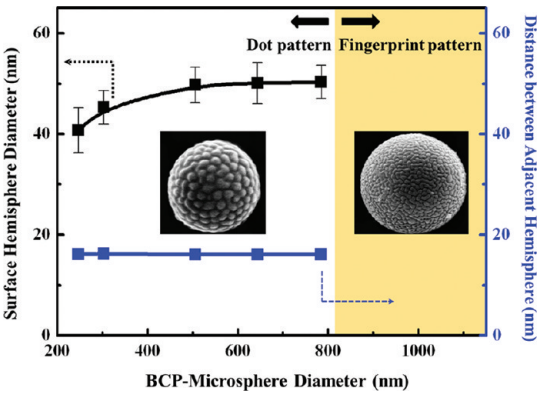

Figure 5. Plot of swollen-surface hemisphere diameter and the distance between adjacent hemispheres as a function of BCP-microsphere diameter. The figure also shows a morphological transition in the microsphere structure from a dot pattern with discrete surface hemispheres to a fingerprint-like pattern with a continuous surface structure as the microsphere diameter increases.

dipole plasmon modes of the Au NPs can be coupled.[52] For example, the UV–vis absorption peak of Au clusters consisting of Au NPs less than 2 nm was observed at a higher wavelength than that of individual Au NPs.[53] Therefore, the red-shifted UV–vis absorption peak indicates that the Au NPs were densely packed in the P4VP domains near the microsphere surfaces. In addition, the presence of Au NPs at the outermost layer of the microspheres was confirmed by energy dispersive X-ray spectrometry (EDX) measurement using a cross-sectioned TEM sample, as shown in Figure S3.

Deeper insight into the morphological transition caused by the addition of Au NPs can be gleaned by examining the structural change of Au-NP-decorated BCP-microspheres as a function of the microsphere diameter. Figure 4 shows SEM images of Au-NP-decorated PS-*b*-P4VP microspheres with different diameters ranging from 250 to 1190 nm. A discrete and regular dotted pattern was observed on small BCP-microspheres, as shown in Figure 4a–d. The surfaces of BCP-microspheres smaller than 800 nm in diameter feature regular arrays of hemispherical protrusions, *i.e.*, raspberry-like structures. However, as the diameter of the microspheres increased, the surface morphology changed, showing a morphological transition from distinct dotted structures to continuous fingerprint-like structures. When the microspheres were larger than 800 nm, their surfaces showed fingerprint-like patterns that may have been caused by the linear fusion of hemispherical protrusions (Figure 4e and f).

To gain deeper insight into the surface structures of the Au-NP-decorated BCP-microspheres, the diameters of the swollen micelles and the distances between adjacent surface structures on the microspheres were measured from SEM images of the microspheres and plotted as a function of the microsphere diameter (Figure 5). Figure 5 shows that the diameter of Au-NP-incorporated P4VP hemispheres on the microsphere surfaces increased from 40 nm as the microsphere diameter increased. However, when the diameter of the microspheres was 800 nm, the hemisphere diameter reached saturation at approximately 50 nm. We suggest that the micelles on the microsphere surface were merged in a different manner depending on the curvature of the microsphere. However, because the distance between the hemispheres was dependent on the length of PS brushes on the P4VP hemispheres, the distance was found constant at approximately 16 nm regardless of the microsphere diameter.

The fluorescence properties of Au-NP-decorated BCP-microspheres are of great importance in understanding the structural behavior of Au NPs in the P4VP domain as well as the morphological transition of the microsphere surface. Of interest is the fluorescence lifetime, which depends mainly on NP size, NP-surrounding interactions, and the concentration of NP fluorophores.[54–56] Therefore, fluorescence lifetime imaging was performed for Au-NP-decorated BCP-microspheres with different diameters and surface structures; the results are presented in Figure S4. The lifetime values for different diameters of microspheres are summarized in Table S1. It was interesting to find that the fluorescence lifetime increased for larger microspheres. Because the Au NPs showed a similar diameter of 1.7 nm regardless of the microsphere

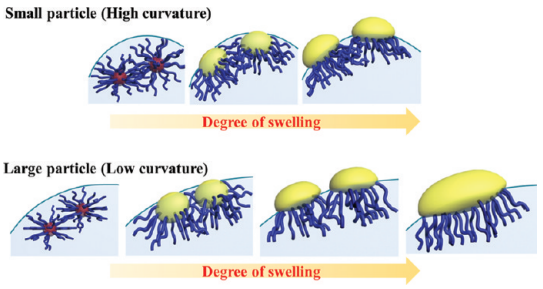

Scheme 2. Schematic diagram of surface-structure evolution on the BCP-microspheres with different diameters as a function of the degree of swelling.

diameter, the increase in the fluorescence lifetime was not due to the changes in the diameter of individual Au NPs. On the contrary, it is well known that fluorophore concentration affects lifetime measurements, and a high concentration of fluorophore typically increases the lifetime through trivial reabsorption processes due to the increased reabsorption probability in the high-concentration region of bulk solution, although the intrinsic lifetime remains unchanged.[55] Therefore, we suggest that fluorescence lifetime increases with increasing microsphere diameter because a larger number of Au NPs can participate in these reabsorption processes within the microsphere.[57] For example, as the microsphere diameter increased from 380 to 810 nm, the P4VP hemisphere on the microsphere surface increased from 40 to 50 nm and thus caused a corresponding increase in the number of Au NPs per P4VP domain, which resulted in the change of the fluorescence lifetime from 2.1 $\pm$ 0.2 to 3.3 $\pm$ 0.2 ns. Interestingly, the fluorescence lifetime further increased to 3.7 ns with the increase in the microsphere diameter from 810 to 1380 nm. We speculate that this was caused by the change in the surface structure from a dotted to a continuous fingerprint pattern, which eventually produced larger numbers of Au NPs per P4VP domain on the surface.

Morphological changes of the sphere surface during swelling and deswelling processes have been investigated in previous studies using buckling or wrinkling theory.[58−60] Diverse patterns are formed by surface wrinkling on a core−shell sphere because the spherical surface buckles as a consequence of energy minimization, and this configuration is energetically favorable. With increasing film stress on the spheres, the protrusions coalesce to reduce the stretching energy and gradually evolve into labyrinth-like patterns. In our experiment, the observed morphologies were quite similar to those of buckled spheres. Moreoever, our results show the formation of BCP-microspheres with different surface structures as a function of the microsphere diameter and thus the surface curvatures. Scheme 2 presents the illustration of the surface-structure evolution on the microspheres as a function of the microsphere diameter. Before the addition of Au precursors, the spherical micelles of PS-*b*-P4VP were

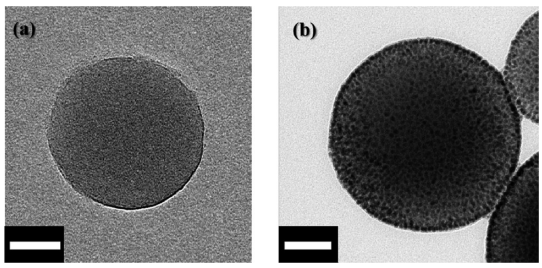

Figure 6. TEM images of a P4VP colloidal particle (a) before and (b) after inserting Au precursors. The P4VP colloidal particle with Au NPs shows a sphere without any undulation on the surface, which is completely different from that of a Au-NP-decorated PS-*b*-P4VP microsphere. In addition, Au NPs were formed homogeneously within the P4VP colloids. Scale bar is 50 nm.

present within the microspheres, in which the PS block is highly swollen with solvent (chloroform) and the P4VP in contrast is collapsed. Therefore, that spherical morphology is retained in the microsphere. Near the surface when the BCP-microspheres is treated with acidic water the P4VP domains swell and burst through the surface coating of PS brushes, forming a mushroom of highly swollen P4VP. We believe that the surface reconstruction of PS-*b*-P4VP structures by Au precursors in acidic water resembles that in thin film geometry by an alcohol reported by Russell *et al.*[61−63] If the curvature of the surface is high enough, the P4VP mushrooms do not touch, thus forming the dot pattern of P4VP structures. However, as the surface curvature decreases, the swollen mushrooms can touch each other and will tend to form continuous half-cylinders. Therefore, the final size of the P4VP surface structure on the microsphere shown in Figure 5 could represent the considerably shrunk one after the deswelling process. Similar curvature-dependent behaviors on the surfaces of emulsions have been reported in a previous study.[64]

As a control experiment, P4VP colloidal particles were prepared under identical conditions to the Au-NP-decorated PS-*b*-P4VP microspheres, but P4VP polymers were used instead of PS-*b*-P4VP polymers. Figure 6 shows TEM images of a P4VP colloidal particle (a) before and (b) after inserting the Au precursors. Unlike the PS-*b*-P4VP microspheres, the P4VP colloidal particles showed no morphological changes upon the addition of Au NPs. In addition, Au NPs were formed uniformly throughout the P4VP colloidal particles. Therefore, it is concluded that the presence of PS-*b*-P4VP spherical micelles is critical to produce Au-NP-decorated BCP-microspheres with controlled surface structures.

Because P4VP polymers can interact favorably with various metal precursors,[6,7] our approach for creating Au-NP-decorated BCP-microspheres can be extended to fabricate hybrid microspheres containing other types of metallic NPs. To this end, metal NP-decorated hybrid BCP-microspheres with controlled surface structures were prepared using two different types of metal precursors, $FeCl_3$ and $HPt_2Cl_6 \cdot 6H_2O$, in which

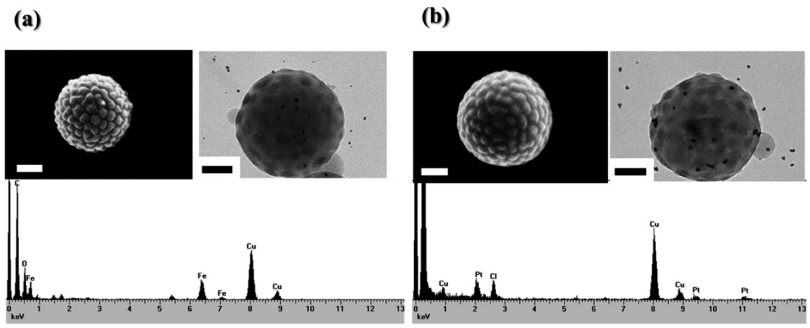

Figure 7. PS-*b*-P4VP microspheres decorated with (a) Fe_xO_y NPs and (b) Pt NPs. Scale bar is 100 nm. Parts (a) and (b) show SEM (top left), TEM (top right), and EDX (bottom) images of Fe_xO_y- and Pt-decorated BCP-microspheres, respectively.

PS-*b*-P4VP can be used as a template to control the location of metal NPs. Both Pt NP- and Fe_xO_y NP-decorated hybrid BCP-microspheres were prepared under conditions identical to Au-NP-decorated BCP-microspheres; however, the Au precursors were replaced with $FeCl_3$ and $HPt_2Cl_6 \cdot 6H_2O$ precursors, respectively. Figure 7 demonstrates the successful fabrication of a PS-*b*-P4VP microsphere decorated with (a) Fe_xO_y and (b) Pt NPs on the surface. The morphology of each microsphere type was carefully observed using FE-SEM and TEM. Analogous to the previously shown system of Au-NP-decorated BCP-microspheres, the surfaces of the microspheres were dramatically transformed from smooth to dot-patterned surfaces upon the addition of the metal precursors, $FeCl_3$ and $HPt_2Cl_6 \cdot 6H_2O$. The formation of Fe_xO_y NPs and Pt NPs on the P4VP domains of the microspheres was observed in the TEM images. In addition, EDX measurement confirmed the presence of Fe_xO_y NPs and Pt NPs in the microspheres. As demonstrated, any precursors that have selective affinities for one block of a BCP could be incorporated for various applications including catalysis, optical sensing, surface-enhanced Raman spectroscopy, meta-materials, and plasmonics.

CONCLUSIONS

In this work, we successfully developed a simple route for producing metal-decorated hybrid "BCP-microspheres" with controlled surface nanostructures. First, microspheres of BCP micelles were prepared through an evaporation-induced self-assembly inside an emulsion. These microspheres can be loaded with metal NPs, through which the metal NPs are incorporated only near the surfaces of the microspheres. Depending on the diameters of the microspheres, unique dotted patterns or fingerprint-like patterns were produced on their surfaces during the infiltration of Au precursors because the P4VP domains near the surface were selectively swollen with Au precursors. We also characterized the optical properties of the Au-NP-decorated BCP-microspheres. The maximum absorption wavelength was observed at approximately 580 nm, indicating that the Au NPs were aggregated or densely packed inside the P4VP domains near the surfaces of the microspheres. Moreover, as the diameter of the microspheres increased, their fluorescence lifetimes were unusually longer than those of smaller microspheres. Furthermore, our approach for Au-NP-decorated BCP-microspheres has been extended to a variety of hybrid microspheres including other metallic NPs, specifically, Fe_xO_y and Pt NPs. Therefore, our approach is envisioned to expand many other applications including catalysts, sensors, and optical/electrical applications, due to their high active surface areas and unique optical/electrical properties.

METHODS

Preparation of BCP-Microspheres Using a PS-*b*-P4VP Polymer. A volume of 0.5 mL of 1 wt % PS-*b*-P4VP (M_n = 262 kg/mol, f_{PS} = 0.76, PDI = 1.14 from Polymer Sources Inc.) polymer solution in chloroform was emulsified in 4.5 mL of distilled water containing 1 wt % Pluronic F108 (PEO-*b*-PPO-*b*-PEO, 15 kg/mol from Aldrich) using a sonicator for 10 min. The aqueous emulsion was diluted with distilled water, and the organic solvent was evaporated at 50 °C under reduced pressure by rotary evaporation. The sample was then annealed at 95 °C for 24 h to obtain the internal structures. The dispersion was washed with deionized (DI) water to remove the remaining surfactants by repeated centrifugations performed at 13 000 rpm for 30 min.

Incorporation of Metallic NPs into BCP-Microspheres. To prepare BCP-microspheres decorated with Au NPs, a Au precursor ($HAuCl_4 \cdot 3H_2O$, purchased from Aldrich) solution was added to a BCP-microsphere dispersion in a 1:1 molar ratio with the P4VP units. The mixture was stirred for 24 h. The mixture was then purified by washing with DI water and repeated centrifugations at 13 000 rpm for 30 min. The products were redispersed in DI water and used for further characterization.

To prepare BCP-microspheres with other types of NPs, $HPt_2Cl_6 \cdot 6H_2O$ and $FeCl_3$ were used as metal precursors; both were purchased from Aldrich. The hybrid microspheres were prepared using the same procedure followed to prepare the Au-NP-decorated BCP-microspheres.

Characterization. Field-emission scanning electron microscopy (FE-SEM, Hitachi S-4800) and transmission electron microscopy (TEM, JEOL 2000FX) were used to observe the surface and internal structures of the metal-decorated BCP-microspheres. To visualize the surface structures of the microspheres

using FE-SEM, the samples were prepared by drop-casting microsphere suspensions onto silicon wafers, which were then washed and sputtered with gold. To investigate the surface structures of the microspheres by TEM, the samples were prepared by dipping TEM grids coated with a 20−30 nm thick carbon film into the microsphere suspensions, followed by drying in air. The prepared samples were exposed to I_2 vapor to selectively stain the P4VP domains of PS-*b*-P4VP. However, after inserting the Au precursor into the PS-*b*-P4VP microspheres, the samples were characterized without staining due to the strong contrast between the Au NPs and polymeric domains. The sizes and distributions of the PS-*b*-P4VP micelles and the Au NPs in the microspheres were determined by analyzing the FE-SEM, TEM, and AFM images. To investigate the internal structures of the microspheres by cross-sectional TEM, the samples were prepared by drop-casting microsphere suspensions onto an epoxy film and allowing the solvent to dry. Then, the epoxy-supported films were cured in an oven at 60 °C for 24 h. The epoxy-supported films were then microtomed with a diamond knife at room temperature into 50 nm slices.

To characterize the optical properties of the Au-NP-decorated BCP-microspheres, UV−vis absorption spectroscopy (Cary 50 Conc UV−vis spectrophotometer) and fluorescence lifetime imaging FLIM were performed. FLIM was performed using an inverted-type scanning confocal microscope (MicroTime-200, Picoquant, Germany) with a 100× objective. A single-mode pulsed diode laser (with a 470 nm output and an instrumental response function of ~96 ps in full-width at half-maximum, a 40 MHz repetition rate, and an average power of less than 1 μW) was used as an excitation source. A dichroic mirror (490 DCXR, AHF), a long-pass filter (HQ500lp, AHF), a 50 μm pinhole, and a single-photon avalanche diode were used to collect the emissions (λ > 500 nm) from Au-NP-decorated samples that were spin-coated onto glass coverslips. Data acquisition was based on a time-correlated single-photon counting technique. Time-resolved fluorescence decay curves were obtained from FLIM images, and fluorescence lifetimes were evaluated according to nonlinear least-squares iterative curve fitting using the SymPhoTime software (ver. 5.1.3).

The presence of Au, Fe_xO_y, and Pt in the hybrid BCP-microspheres was confirmed by EDX measurement (JEOL). The samples were prepared using the same procedure as that used to prepare the samples for TEM but were not stained.

Conflict of Interest: The authors declare no competing financial interest.

Acknowledgment. This research was supported by the Korea Research Foundation Grant, funded by the Korean Government (2011-0017943, 2011-0027240, 2011-0027518, 2009-0082451). The authors thank Prof. Edward J. Kramer for valuable discussions.

Supporting Information Available: Additional NMR, AFM, EDX, and FILM data. This material is available free of charge *via* the Internet at http://pubs.acs.org.

REFERENCES AND NOTES

1. Jeon, S. J.; Yi, G. R.; Yang, S. M. Cooperative Assembly of Block Copolymers with Deformable Interfaces: Toward Nanostructured Particles. *Adv. Mater.* **2008**, *20*, 4103–4108.
2. Yabu, H.; Higuchi, T.; Shimomura, M. Unique Phase-Separation Structures of Block-Copolymer Nanoparticles. *Adv. Mater.* **2005**, *17*, 2062–2065.
3. Jeon, S. J.; Yi, G. R.; Koo, C. M.; Yang, S. M. Nanostructures inside Colloidal Particles of Block Copolymer/Homopolymer Blends. *Macromolecules* **2007**, *40*, 8430–8439.
4. Kim, B. J.; Bang, J.; Hawker, C. J.; Chiu, J. J.; Pine, D. J.; Jang, S. G.; Yang, S. M.; Kramer, E. J. Creating Surfactant Nanoparticles for Block Copolymer Composites through Surface Chemistry. *Langmuir* **2007**, *23*, 12693–12703.
5. Bockstaller, M. R.; Lapetnikov, Y.; Margel, S.; Thomas, E. L. Size-Selective Organization of Enthalpic Compatibilized Nanocrystals in Ternary Block Copolymer/Particle Mixtures. *J. Am. Chem. Soc.* **2003**, *125*, 5276–5277.
6. Hayward, R. C.; Chmelka, B. F.; Kramer, E. J. Crosslinked Poly(styrene)-Block-Poly(2-vinylpyridine) Thin Films as Swellable Templates for Mesostructured Silica and Titania. *Adv. Mater.* **2005**, *17*, 2591–2595.
7. Chai, J.; Wang, D.; Fan, X. N.; Buriak, J. M. Assembly of Aligned Linear Metallic Patterns on Silicon. *Nat. Nanotechnol.* **2007**, *2*, 500–506.
8. Chiu, J. J.; Kim, B. J.; Kramer, E. J.; Pine, D. J. Control of Nanoparticle Location in Block Copolymers. *J. Am. Chem. Soc.* **2005**, *127*, 5036–5037.
9. Boontongkong, Y.; Cohen, R. E. Cavitated Block Copolymer Micellar Thin Films: Lateral Arrays of Open Nanoreactors. *Macromolecules* **2002**, *35*, 3647–3652.
10. Kim, B. J.; Chiu, J. J.; Yi, G. R.; Pine, D. J.; Kramer, E. J. Nanoparticle-Induced Phase Transitions in Diblock-Copolymer Films. *Adv. Mater.* **2005**, *17*, 2618–2622.
11. Kane, R. S.; Cohen, R. E.; Silbey, R. Synthesis of Doped ZnS Nanoclusters within Block Copolymer Nanoreactors. *Chem. Mater.* **1999**, *11*, 90–93.
12. Misner, M. J.; Skaff, H.; Emrick, T.; Russell, T. P. Directed Deposition of Nanoparticles Using Diblock Copolymer Templates. *Adv. Mater.* **2003**, *15*, 221–224.
13. Sankaran, V.; Yue, J.; Cohen, R. E.; Schrock, R. R.; Silbey, R. J. Synthesis of Zinc-Sulfide Clusters and Zinc Particles within Microphase-Separated Domains of Organometallic Block-Copolymers. *Chem. Mater.* **1993**, *5*, 1133–1142.
14. Spatz, J.; Mossmer, S.; Moller, M.; Kocher, M.; Neher, D.; Wegner, G. Controlled Mineralization and Assembly of Hydrolysis-Based Nanoparticles in Organic Solvents Combining Polymer Micelles and Microwave Techniques. *Adv. Mater.* **1998**, *10*, 473–475.
15. Lopes, W. A.; Jaeger, H. M. Hierarchical Self-Assembly of Metal Nanostructures on Diblock Copolymer Scaffolds. *Nature* **2001**, *414*, 735–738.
16. Tsutsumi, K.; Funaki, Y.; Hirokawa, Y.; Hashimoto, T. Selective Incorporation of Palladium Nanoparticles into Microphase-Separated Domains of Poly(2-vinylpyridine)-Block-Polyisoprene. *Langmuir* **1999**, *15*, 5200–5203.
17. Sohn, B. H.; Seo, B. H. Fabrication of the Multilayered Nanostructure of Alternating Polymers and Gold Nanoparticles with Thin Films of Self-Assembling Diblock Copolymers. *Chem. Mater.* **2001**, *13*, 1752–1757.
18. Paek, K.; Chung, S.; Cho, C. H.; Kim, B. J. Fluorescent and pH-responsive Diblock Copolymer-Coated Core-Shell CdSe/ZnS Particles for a Color-Displaying, Ratiometric pH Sensor. *Chem. Commun.* **2011**, *47*, 10272–10274.
19. Lim, J.; Yang, H.; Paek, K.; Cho, C. H.; Kim, S.; Bang, J.; Kim, B. J. "Click" Synthesis of Thermally Stable Au Nanoparticles with Highly Grafted Polymer Shell and Control of Their Behavior in Polymer Matrix. *J. Polym. Sci. A: Polym. Chem.* **2011**, *49*, 3464–3474.
20. Yoo, M.; Kim, S.; Lim, J.; Kramer, E. J.; Hawker, C. J.; Kim, B. J.; Bang, J. Facile Synthesis of Thermally Stable Core-Shell Gold Nanoparticles *via* Photo-Cross-Linkable Polymeric Ligands. *Macromolecules* **2010**, *43*, 3570–3575.
21. Jang, S. G.; Khan, A.; Dimitriou, M. D.; Kim, B. J.; Lynd, N. A.; Kramer, E. J.; Hawker, C. J. Synthesis of Thermally Stable Au-Core/Pt-Shell Nanoparticles and Their Segregation Behavior in Diblock Copolymer Mixtures. *Soft Matter* **2011**, *7*, 6255–6263.
22. Zhao, Y.; Thorkelsson, K.; Mastroianni, A. J.; Schilling, T.; Luther, J. M.; Rancatore, B. J.; Matsunaga, K.; Jinnai, H.; Wu, Y.; Poulsen, D.; *et al.* Small-Molecule-Directed Nanoparticle Assembly towards Stimuli-Responsive Nanocomposites. *Nat. Mater.* **2009**, *8*, 979–985.
23. Lin, Y.; Daga, V. K.; Anderson, E. R.; Gido, S. P.; Watkins, J. J. Nanoparticle-Driven Assembly of Block Copolymers: A Simple Route to Ordered Hybrid Materials. *J. Am. Chem. Soc.* **2011**, *133*, 6513–6516.
24. Li, L.; Miesch, C.; Sudeep, P. K.; Balazs, A. C.; Emrick, T.; Russell, T. P.; Hayward, R. C. Kinetically Trapped Co-Continuous Polymer Morphologies through Intraphase Gelation of Nanoparticles. *Nano Lett.* **2011**, *11*, 1997–2003.

25. Listak, J.; Bockstaller, M. R. Stabilization of Grain Boundary Morphologies in Lamellar Block Copolymer/Nanoparticle Blends. *Macromolecules* **2006**, *39*, 5820–5825.
26. Spontak, R. J.; Shankar, R.; Bowman, M. K.; Krishnan, A. S.; Hamersky, M. W.; Samseth, J.; Bockstaller, M. R.; Rasmussen, K. O. Selectivity- and Size-Induced Segregation of Molecular and Nanoscale Species in Microphase-Ordered Triblock Copolymers. *Nano Lett.* **2006**, *6*, 2115–2120.
27. Chen, X. C.; Green, P. F. Structure of Thin Film Polymer/Nanoparticle Systems: Polystyrene (PS) Coated-Au Nanoparticle/Tetramethyl Bisphenol-A Polycarbonate Mixtures (TMPC). *Soft Matter* **2011**, *7*, 1192–1198.
28. Chung, H.; Ohno, K.; Fukuda, T.; Composto, R. J. Self-Regulated Structures in Nanocomposites by Directed Nanoparticle Assembly. *Nano Lett.* **2005**, *5*, 1878–1882.
29. Kim, B. J.; Bang, J.; Hawker, C. J.; Kramer, E. J. Effect of Areal Chain Density on the Location of Polymer-Modified Gold Nanoparticles in a Block Copolymer Template. *Macromolecules* **2006**, *39*, 4108–4114.
30. Jeon, S. J.; Kim, B. J.; Petrie, J. D.; Jang, S. G.; Kramer, E. J.; Pine, D. J.; Yi, G. R.; Yang, S. M. Hierarchically Structured Colloids of Diblock Copolymers and Au Nanoparticles. *Chem. Mater.* **2009**, *21*, 3739–3741.
31. Kang, D. J.; Kwon, T.; Kim, M. P.; Cho, C.-H.; Jung, H.; Bang, J.; Kim, B. J. Creating Opal-Templated Continuous Conducting Polymer Films with Ultralow Percolation Thresholds Using Thermally Stable Nanoparticles. *ACS Nano* **2011**, *5*, 9017–9027.
32. Kwon, T.; Kim, T.; Fathilah, A.; Kang, D. J.; Bang, J.; Lee, W.; Kim, B. J. Size Controlled Polymer Coated Nanoparticles as Efficient Compatibilizers for Polymer Blends. *Macromolecules* **2011**, *44*, 9852–9862.
33. Jang, S. G.; Kramer, E. J.; Hawker, C. J. Controlled Supramolecular Assembly of Micelle-like Gold Nanoparticles in PS-b-P2VP Diblock Copolymers *via* Hydrogen Bonding. *J. Am. Chem. Soc.* **2011**, *133*, 16986–16996.
34. Koh, H. D.; Park, S.; Russell, T. P. Fabrication of Pt/Au Concentric Spheres from Triblock Copolymer. *ACS Nano* **2010**, *4*, 1124–1130.
35. Koh, H. D.; Kang, N. G.; Lee, J. S. Fabrication of an Open Au/Nanoporous Film by Water-in-Oil Emulsion-Induced Block Copolymer Micelles. *Langmuir* **2007**, *23*, 12817–12820.
36. Li, B.; Lu, G.; Zhou, X.; Cao, X.; Boey, F.; Zhang, H. Controlled Assembly of Gold Nanoparticles and Graphene Oxide Sheets on Dip Pen Nanolithography-Generated Templates. *Langmuir* **2009**, *25*, 10455–10458.
37. Yoo, H.; Park, S. The Fabrication of Highly Ordered Block Copolymer Micellar Arrays: Control of the Separation Distances of Silicon Oxide Dots. *Nanotechnology* **2010**, *21*, 245304.
38. Cong, Y.; Zhang, Z.; Fu, J.; Li, J.; Han, Y. Water-Induced Morphology Evolution of Block Copolymer Micellar Thin Films. *Polymer* **2005**, *46*, 5377–5384.
39. Ningrum, E. O.; Lin, W. T.; Lo, C. T. The Nanostructure and Dewetting of Block Copolymer Thin Films Annealed in Different Neutral Solvents. *Polym. Eng. Sci.* **2011**, *51*, 1339–1346.
40. Maki-Ontto, R.; de Moel, K.; de Odorico, W.; Ruokolainen, J.; Stamm, M.; ten Brinke, G.; Ikkala, O. "Hairy Tubes": Mesoporous Materials Containing Hollow Self-Organized Cylinders with Polymer Brushes at the Walls. *Adv. Mater.* **2001**, *13*, 117–121.
41. Agrawal, M.; Rubio-Retama, J.; Zafeiropoulos, N. E.; Gaponik, N.; Gupta, S.; Cimrova, V.; Lesnyak, V.; Lopez-Cabarcos, E.; Tzavalas, S.; Rojas-Reyna, R.; *et al.* Switchable Photoluminescence of CdTe Nanocrystals by Temperature-Responsive Microgels. *Langmuir* **2008**, *24*, 9820–9824.
42. Ming, W.; Wu, D.; van Benthem, R.; de With, G. Superhydrophobic Films from Raspberry-like Particles. *Nano Lett.* **2005**, *5*, 2298–2301.
43. Guan, N.; Xu, J.; Wang, L.; Sun, D. One-Step Synthesis of Amine-Functionalized Thermo-Responsive Magnetite Nanoparticles and Single-Crystal Hollow Structures. *Colloids Surf., A* **2009**, *346*, 221–228.
44. Isenbugel, K.; Gehrke, Y.; Ritter, H. Evaporation-Driven Self-Assembly of Colloidal Silica Dispersion: New Insights on Janus Particles. *Macromol. Rapid Commun.* **2012**, *33*, 41–46.
45. Love, J. C.; Estroff, L. A.; Kriebel, J. K.; Nuzzo, R. G.; Whitesides, G. M. Self-Assembled Monolayers of Thiolates on Metals as a Form of Nanotechnology. *Chem. Rev.* **2005**, *105*, 1103–1169.
46. Cheng, F.; Zhang, K.; Chen, D.; Zhu, L.; Jiang, M. Self-Assembly of Heteroarms Core-Shell Polymeric Nanoparticles (HCPNs) and Templated Synthesis of Gold Nanoparticles within HCPNs and the Superparticles. *Macromolecules* **2009**, *42*, 7108–7113.
47. Huang, R.; Chen, D.; Jiang, M. Polymeric Core-Shell Stars with a Novel Fluorescent, Cross-Linked and Swollen Core: Their Efficient One-Step Preparation, Further Self-Assembly into Superparticles and Application as a Chemosensor. *J. Mater. Chem.* **2010**, *20*, 9988–9994.
48. Link, S.; El-Sayed, M. A. Size and Temperature Dependence of the Plasmon Absorption of Colloidal Gold Nanoparticles. *J. Phys. Chem. B* **1999**, *103*, 4212–4217.
49. Liz-Marzan, L. M.; Giersig, M.; Mulvaney, P. Synthesis of Nanosized Gold-Silica Core-Shell Particles. *Langmuir* **1996**, *12*, 4329–4335.
50. Alvarez, M. M.; Khoury, J. T.; Schaaff, T. G.; Shafigullin, M. N.; Vezmar, I.; Whetten, R. L. Optical Absorption Spectra of Nanocrystal Gold Molecules. *J. Phys. Chem. B* **1997**, *101*, 3706–3712.
51. Liu, Y. C.; Lin, L. H.; Chiu, W. H. Size-Controlled Synthesis of Gold Nanoparticles from Bulk Gold Substrates by Sonoelectrochemical Methods. *J. Phys. Chem. B* **2004**, *108*, 19237–19240.
52. Ung, T.; Liz-Marzan, L. M.; Mulvaney, P. Optical Properties of Thin Films of Au@SiO_2 Particles. *J. Phys. Chem. B* **2001**, *105*, 3441–3452.
53. Polavarapu, L.; Manna, M.; Xu, Q. H. Biocompatible Glutathione Capped Gold Clusters as One- and Two-Photon Excitation Fluorescence Contrast Agents for Live Cells Imaging. *Nanoscale* **2011**, *3*, 429–434.
54. Seelig, J.; Leslie, K.; Renn, A.; Kuhn, S.; Jacobsen, V.; van de Corput, M.; Wyman, C.; Sandoghdar, V. Nanoparticle-Induced Fluorescence Lifetime Modification as Nanoscopic Ruler: Demonstration at the Single Molecule Level. *Nano Lett.* **2007**, *7*, 685–689.
55. Selanger, K. A.; Falnes, J.; Sikkeland, T. Fluorescence Lifetime Studies of Rhodamine 6g in Methanol. *J. Phys. Chem.* **1977**, *81*, 1960–1963.
56. Chhabra, R.; Sharma, J.; Wang, H. N.; Zou, S. L.; Lin, S.; Yan, H.; Lindsay, S.; Liu, Y. Distance-Dependent Interactions between Gold Nanoparticles and Fluorescent Molecules with DNA as Tunable Spacers. *Nanotechnology* **2009**, *20*, 485201.
57. Berezin, M. Y.; Achilefu, S. Fluorescence Lifetime Measurements and Biological Imaging. *Chem. Rev.* **2010**, *110*, 2641–2684.
58. Yin, J.; Cao, Z.; Li, C.; Sheinman, I.; Chen, X. Stress-Driven Buckling Patterns in Spheroidal Core/Shell Structures. *Proc. Natl. Acad. Sci. U. S. A.* **2008**, *105*, 19132–19135.
59. Cao, G.; Chen, X.; Li, C.; Ji, A.; Cao, Z. Self-Assembled Triangular and Labyrinth Buckling Patterns of Thin Films on Spherical Substrates. *Phys. Rev. Lett.* **2008**, *100*, 036102.
60. Li, B.; Jia, F.; Cao, Y. P.; Feng, X. Q.; Gao, H. J. Surface Wrinkling Patterns on a Core-Shell Soft Sphere. *Phys. Rev. Lett.* **2011**, *106*, 234301.
61. Cho, H.; Park, H.; Russell, T. P.; Park, S. Precise Placements of Metal Nanoparticles from Reversible Block Copolymer Nanostructures. *J. Mater. Chem.* **2010**, *20*, 5047–5051.
62. Park, S.; Wang, J. Y.; Kim, B.; Xu, J.; Russell, T. P. A Simple Route to Highly Oriented and Ordered Nanoporous Block Copolymer Templates. *ACS Nano* **2008**, *2*, 766–772.
63. Park, S.; Kim, B.; Wang, J. Y.; Russell, T. P. Fabrication of Highly Ordered Silicon Oxide Dots and Stripes from Block Copolymer Thin Films. *Adv. Mater.* **2008**, *20*, 681–685.
64. Chang, C. B.; Knobler, C. M.; Gelbart, W. M.; Mason, T. G. Curvature Dependence of Viral Protein Structures on Encapsidated Nanoemulsion Droplets. *ACS Nano* **2008**, *2*, 281–286.